Sensitivity of surface heat and moisture fluxes due to topographic slope and azimuth

Norman L. Miller

Lawrence Livermore National Laboratory, University of California, Livermore, California

Abstract. Current surface vegetation atmospheric transfer (SVAT) models neglect the effects of surface slope and azimuth. There are significant subgrid differences in topographic features at the subgrid scales to which processes such as latent and sensible heating fluxes are sensitive. This study indicates the sensitivity of these processes due to sloping surfaces of varying azimuth (clockwise horizontal direction from north). A dynamically adaptive gridding system is implemented to determine subgrids based on surface slope and azimuth. A topographic index which accounts for four surface azimuth and five slope increments defines 21 characteristic types, including flat horizontal surfaces. A synthetic 10 km x 10 km watershed at latitude 38°N and with a fixed diurnal cycle provides input for the surface temperature. Two fine grid meshes, 1.0 km x 1.0 km and 2 km x 2 km, are embedded within the larger-scale cell. Digital elevation data representing an area near Lake Tahoe, California, is also used in this sensitivity study of surface heat and moisture fluxes due to topographic forcing of incident radiation. A homogeneity test determines the minimum number of fine scale cells with matching characteristics and shared boundaries (but not strictly shared points) and forms groups of cells which represent regions of similar topographic characteristics. When the homogeneity test is set to 100% accuracy, there is a 72% reduction from individual fine grid cells to similar groups, while at 60% accuracy there is an 80% reduction, and at 10% accuracy there is a 99% reduction. Each group computes a SVAT with the group defined characteristic topography. A set of test cases using the Biosphere-Atmosphere Transfer Scheme (Dickinson et al., 1986) is presented for north, south, east, and west facing 10° slopes with surfaces under dry and saturated conditions. The resulting latent heat fluxes are shown for grasslands and evergreen forests under dry and saturated conditions and for the synthetic watershed at varying degrees of accuracy. The Sierra topography is assumed to be all evergreen vegetation and dry. This study indicates that flat horizontal surfaces overpredict diurnally integrated, areally weighted sensible heat fluxes by 5 to 10% and latent heat fluxes by 1 to 2%.

Introduction

The surface of the Earth is composed of nonuniform terrain. Valleys, hill slopes, and mountains range in size from a few meters to hundreds of meters in height over a distance of a few kilometers. Terrain partially controls the amount of incident radiation available at the surface and in turn partially controls regional vegetation, hydrology, and ecology. A more complete treatment of the Earth climate system requires parameterizations of detailed descriptions of land surface processes.

The effect of subgrid topography on surface processes has been addressed recently by a number of researchers. *Mahrt* [1987] has formulated grid-averaged surface fluxes based on the assumption of idealized subgrid spatial distributions of the Richardson number. *Andre et al.* [1990] have estimated heat and moisture fluxes over heterogeneous terrain from the Hapex-Mobilhy experiments. *Avissar and Pielke* [1989] and *Avissar* [1991] have shown that surface heat and momentum depend nonlinearly on topographic heterogeneity. They proposed a statistical-dynamical parameterization for subgrid-

scale forcing of terrain on energy fluxes using area-weighted average flux values with normal distributions. *Pielke et al.* [1991] have modeled the nonlinear influence of land use over flat terrain, while *Lee et al.* [1991] have investigated the spatial representation of land surface characteristics with an atmospheric model using spectral analysis [*Dalu and Pielke*, 1991] to fractionally weight contributions of different spatial scales. *Pielke et al.* [1993] formulated a parameterization of landscape variability for general circulation models using a parameterization based on their spectral analysis.

Land surface models (LSMs) have typically been coupled with atmospheric models (AMs) on the basis of grid point by grid point matching or using a fractional percentage. This type of mapping between AMs and LSMs will smooth out subgrid processes at the surface, omitting significant details that may be necessary for an accurate simulation of climate change.

Coupling fine grid LSMs to medium resolution AMs has been proposed. However, this will become computationally prohibitive as more detailed LSMs are implemented. Fixed input surface characteristic maps of vegetation, soils, and topography cannot accommodate time dependent changes that occur while a climate simulation is running. For example, regions of simulated deforestation must be properly accounted for and updated to provide an accurate independent calculation of the resulting albedo, surface roughness, momentum flux, and evapotransporation. The ability of a climate model to determine the feedback and sensitivities of atmospheric

forcings on the land surface and in turn the resulting effects of land surface fluxes on the atmospheric boundary layer depends critically on the accuracy with which subgrid processes are computed.

Accurate land surface - atmosphere interactions, based on LSMs driven in part by atmospheric state variables, may require the terrain to be viewed as homogeneous sub-regions of slope and azimuth, particularly over complex terrain. Processes associated with net solar radiation and hydrology are sensitive to the degree to which the surface slope and azimuth are approximated. Several surface processes are a function of the amount of incident solar radiation which depends on the zenith angle, surface slope angle, and azimuth angle, where azimuth angle is defined here as the clockwise horizontal angle from north.

As an approach to bridging the spatial spectrum, horizontal length scales ranging from 1 km up to 100 km, a homogeneity testing and grouping scheme has been formulated [*Miller* 1993a]. This scheme minimizes computing requirements while maintaining a high degree of spatial accuracy. A variable threshold criterion establishes the degree of accuracy in reproducing the surface characteristics. This scheme is discussed in the appendix of this paper. The overall intent here is to present this homogeneity technique for resolving regions of homogeneous slope and azimuth and to show its effects on the latent and sensible heat fluxes. The next section discusses the formation of a topographic characteristic; this is followed by computed sensitivities of surface heat and moisture fluxes for a synthetic watershed at two spatial resolutions and for topography near Lake Tahoe, California.

Methods

Formation of a Slope and Azimuth Characteristic for a Single LSM Cell

Slope and azimuth for each LSM cell is computed from a biquadratic interpolation spline [*DeBoor* 1978] using the surrounding sixteen grid points. This interpolation provides a cell height (z) about its centroid, derivatives of elevation in both the south to north direction (dy/dz) and the west to east direction (dx/dz), and information on the goodness of fit. The angle between the vertical and the normal to each LSM cell (the steepest descent along a gradient slope) is given as

$$\beta = \cos^{-1}[(1.0 + dx/dz^2 + dy/dz^2)^{-\frac{1}{2}}],$$

and the angle between north and the steepest descent vector (azimuth) is expressed as

$$\phi = \pi/2 - \tan^{-1}[(dx/dz)/(dy/dz)] .$$

Figure 1 shows β and ϕ for a single surface cell.

A slope/azimuth characteristic based on $\tan\beta$ and ϕ was created with 21 categories. Flat surfaces were set to 0, azimuth was given double digit values, and slope was given incremental single digit values. The azimuth was divided up into four sectors; that is, if ϕ is greater than 315° and less than or equal to 45°, then a value of 10 is assigned; if ϕ is greater than 45° but less than or equal to 135° then a value of 20 is assigned; if ϕ is greater than 135° and less than or equal to 225° then a value of 30 is given; and if ϕ is greater than 225° and less than or equal to 315° a value of 40 is given. The second digit is defined by increments of β and ranges between
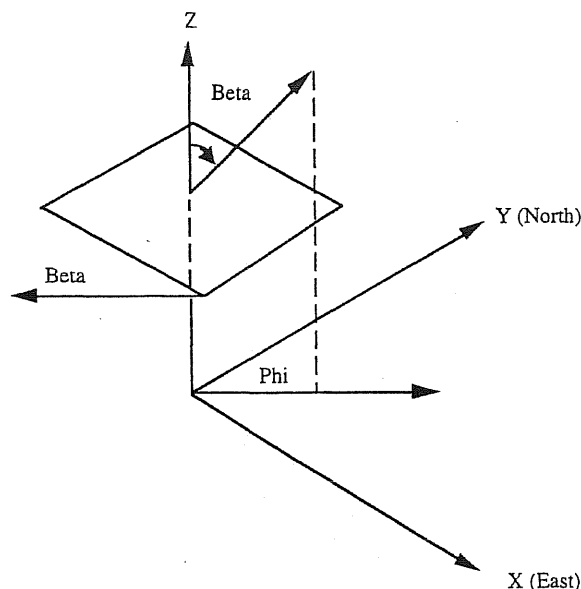

Figure 1. Slope angle (β) and azimuthal angle (ϕ) for a single land surface cell.

less than 1° and greater than 25°. These two degrees of freedom which determine the topographic characteristic index are a first approximation set of increments and are shown in Figure 2. The chosen increments may be expanded to provide greater detail depending on future sensitivity tests and applications.

Homogeneous Groups of Similar Terrain for a Synthetic Watershed

A synthetic terrain with symmetry in both the north to south and the east to west directions has been chosen as an initial sensitivity testing surface with the application of the homogeneity test (Figure 3). This simple 10 km x 10 km watershed is composed of 100 surface cells that are each 1 km x 1 km. The terrain has north sloping and south sloping surfaces that level out onto a plateau; the east and west slopes drop off and away from the flat surface. This simple surface was chosen because mountainous watersheds tend to have similar features, so a sensitivity study on this configuration will yield similar results. The homogeneity scheme is coupled to the LSM developed by *Dickinson et al.* [1986], the Biosphere Atmosphere Transfer Scheme (BATS), to indicate the resulting latent and sensible heat fluxes.

The longitudinal and latitudinal derivatives (dx/dz, dy/dz) are computed for the 100 surface cells with the critical threshold set to 1.0 (Table 1a and b). The lower left corner corresponds to the southwest and the upper right corresponds to the northeast. The positive slope in x indicates the increasing surface change with height; this increases from the west to the center which is a plateau, and then decreases to the east. Similarly, for the y derivative, there is a decreasing slope from the south down to the plateau region and then an increase toward the northern edge of the domain.

This synthetic terrain is disaggregated into groups of similar slope and azimuth via the homogeneity test. Figure 4a illustrates the decomposition and formation of homogenous topographical groups for critical threshold values, ε, ranging
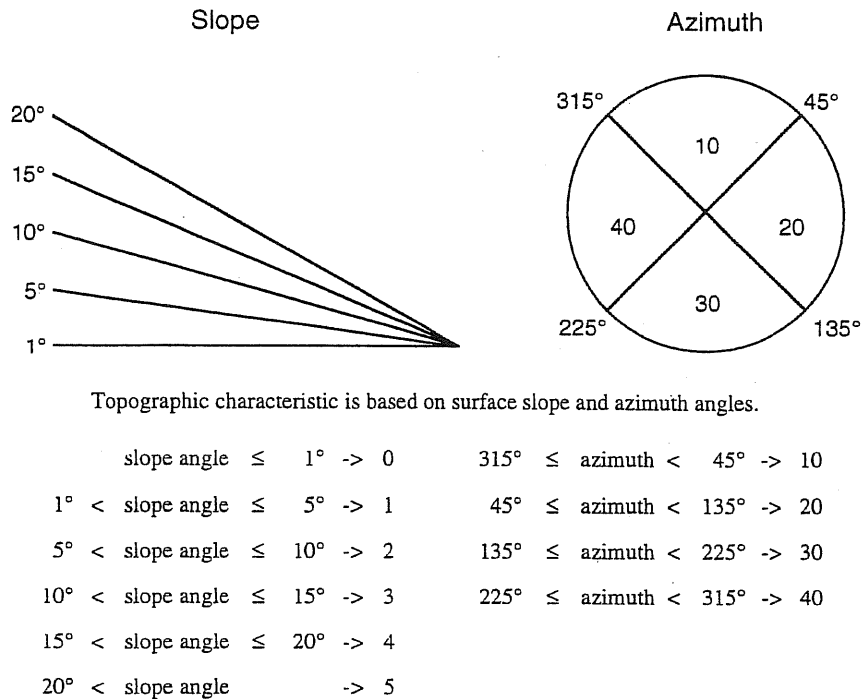
Slope   Azimuth

Topographic characteristic is based on surface slope and azimuth angles.

	slope angle	$\leq$	1°	-> 0		315°	$\leq$	azimuth	<	45°	-> 10
1° <	slope angle	$\leq$	5°	-> 1		45°	$\leq$	azimuth	<	135°	-> 20
5° <	slope angle	$\leq$	10°	-> 2		135°	$\leq$	azimuth	<	225°	-> 30
10° <	slope angle	$\leq$	15°	-> 3		225°	$\leq$	azimuth	<	315°	-> 40
15° <	slope angle	$\leq$	20°	-> 4							
20° <	slope angle			-> 5							

Figure 2. Formulation of a topographic slope/azimuth characteristic index as discussed in the text.

from 0.0 to 1.0. Figure 4b indicates the corresponding slope/azimuth characteristic for each of the groups that are identified in Figure 4a. At $\varepsilon = 0.4$ only four groups are required; however, the accuracy is very low. This level may be satisfactory for certain coarse large scale applications. At $\varepsilon = 0.8$ there is 100% accuracy and 21 groups; this does not vary as ε increases to 1.0.

Results and Discussion

Incident Solar Radiation Response to Slope and Azimuth

Land surfaces receive direct incident solar radiation as a function of the declination angle, slope angle, and azimuth angle. To begin to quantify the effect of topography, four surfaces each with a 10° slope (northward, southward, eastward, and westward) and one with a flat horizontal surface were used. These five slopes correspond to groups 1, 7, 12, 3, and 6 in Figure 4a, respectively. Each of the five surfaces were specified as having tall grass vegetation properties and then evergreen woodland properties with constant soil depths. A specified atmospheric forcing was applied with constant winds of 3.6 m/s, surface pressure of 1000 mbar, and no precipitation except for the saturated case. The atmospheric temperature was specified as a sinusoidally diurnal atmospheric temperature with a mean value of 18° C and a deviation of 5° C. The incident solar radiation is based on the actinometric formulations for sloping surfaces as provided by *Kondrat'yev* [1965]. These atmospheric forcings are used throughout this study unless specified otherwise.

An incident solar radiation plot for June 6 is shown in Figure 5. The five surfaces receive varying amounts of incident

solar radiation throughout the day. The curves shown here are in agreement with Figure 7 of *Avissar and Pielke* [1989]. Incident solar radiation forces the surface fluxes as shown in figures 6a-6d. Figures 6a and 6b are the sensible heat fluxes and latent heat fluxes over tall grass, respectively. Figures 6c and 6d are the sensible heat fluxes and latent heat fluxes over evergreen woodland. For tall grass at noon, the sensible heat flux ranges from 297 to 350 W/m² and the latent heat flux ranges from 97 to 99 W/m², where the north facing slope
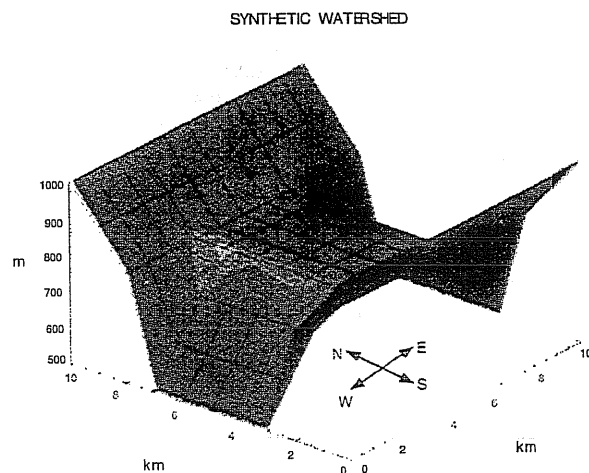
SYNTHETIC WATERSHED

Figure 3. Synthetic terrain with symmetry about the north-south axis and also about the east-west axis. The 100 land surface cells are each 1 km².

Table 1a. Longitudinal Derivatives of the Synthetic Terrain dx/dz

0.006	0.006	0.007	-0.001	0.000	0.000	0.001	-0.007	-0.006	-0.006
-0.018	-0.017	-0.021	0.004	-0.001	0.001	-0.004	0.021	0.017	0.018
0.100	0.097	0.121	-0.021	0.004	-0.004	0.021	-0.121	-0.097	-0.100
0.217	0.210	0.262	-0.045	0.009	-0.009	0.045	-0.262	-0.210	-0.217
0.198	0.191	0.238	-0.041	0.008	-0.008	0.041	-0.238	-0.191	-0.198
0.198	0.191	0.238	-0.041	0.008	-0.008	0.041	-0.238	-0.191	-0.198
0.217	0.210	0.262	-0.045	0.009	-0.009	0.045	-0.262	-0.210	-0.217
0.100	0.097	0.121	-0.021	0.004	-0.004	0.021	-0.121	-0.097	-0.100
-0.018	-0.017	-0.021	0.004	-0.001	0.001	-0.004	0.021	0.017	0.018
0.006	0.006	0.007	-0.001	0.000	0.000	0.001	-0.007	-0.006	-0.006

Longitudinal derivative in x at cell center.

Table 1b. Latitudinal Derivatives of the Synthetic Terrain dy/dz

0.200	0.200	0.200	0.200	0.20	0.200	0.200	0.200	0.200	0.200
0.123	0.169	0.220	0.244	0.240	0.240	0.244	0.220	0.169	0.123
0.664	0.386	0.079	-0.062	-0.038	-0.038	-0.062	0.079	0.386	0.664
-0.115	-0.067	-0.014	0.011	0.007	0.007	0.011	-0.014	-0.067	-0.115
0.023	0.013	0.003	-0.002	-0.001	-0.001	-0.002	0.003	0.013	0.023
-0.023	-0.013	-0.003	0.002	0.001	0.001	0.002	-0.003	-0.013	-0.023
0.115	0.067	0.014	-0.011	-0.007	-0.007	-0.011	0.014	0.067	0.115
-0.664	-0.386	-0.079	0.062	0.038	0.038	0.062	-0.079	-0.386	-0.664
-0.123	-0.169	-0.220	-0.244	-0.240	-0.240	-0.244	-0.220	-0.169	-0.123
-0.200	-0.200	-0.200	-0.200	-0.200	-0.200	-0.200	-0.200	-0.200	-0.200

Latitudinal derivative in y at cell center. The upper left corners represent the northwest and the lower right corners represent the southeast of this region.

(south -> north) has the lowest value and the south facing slope (north -> south) has the highest value. For evergreen woodland at noon, the sensible heat flux ranges from 163 to 210 W/m^2 and the latent heat flux ranges from 270 to 278 W/m^2. Throughout the day this range varies and is most pronounced at low sun angles.

A normalized ratio of the sensible heat fluxes to the flat surface under dry conditions, indicates that the sensible heat fluxes are the most sensitive to slope angle and azimuth. The 0600 UT westward slope indicates a -3.58 percent decrease from the flat surface value and the 1800 UT eastward slope indicates a -4.19 percent decrease. The southward slope value ranges from 2.25 percent at 0600 UT to 0.04 percent at 1800 UT. The normalized northward sensible heat flux ranges from -0.30 percent at 0600 UT to a maximum of 2.08 percent at 1800 UT. These large differences in the 0600 and 1800 UT values may be deceiving as they are the ratio of two small values, whereas smaller noon ratios are based on much larger absolute values.

When the surface is saturated, the normalized sensible heat flux is found to be extremely large early in the morning and then again near sunset. The most significant time is at 0900 UT where the normalized southward sensible heat flux is 2.56 percent greater than the flat surface value, the northward value is -4.27 percent, the westward is -18.38 percent, and the eastward is 14.84 percent. These values are due to the early morning solar heating on the eastward slope causing an increased sensible heat flux; the reverse is true for the westward slope.

The normalized latent heat flux remains between 0.98 and 1.02 percent for all of the slopes during the diurnal period for both dry and saturated conditions. This is true for the given set of climatic conditions and latitude. However, as the specific humidity increases or the declination decreases or the latitude increases, there will be a greater range in the normalized latent heat flux.

Distribution of Diurnally Integrated Surface Fluxes for the Resulting Groups

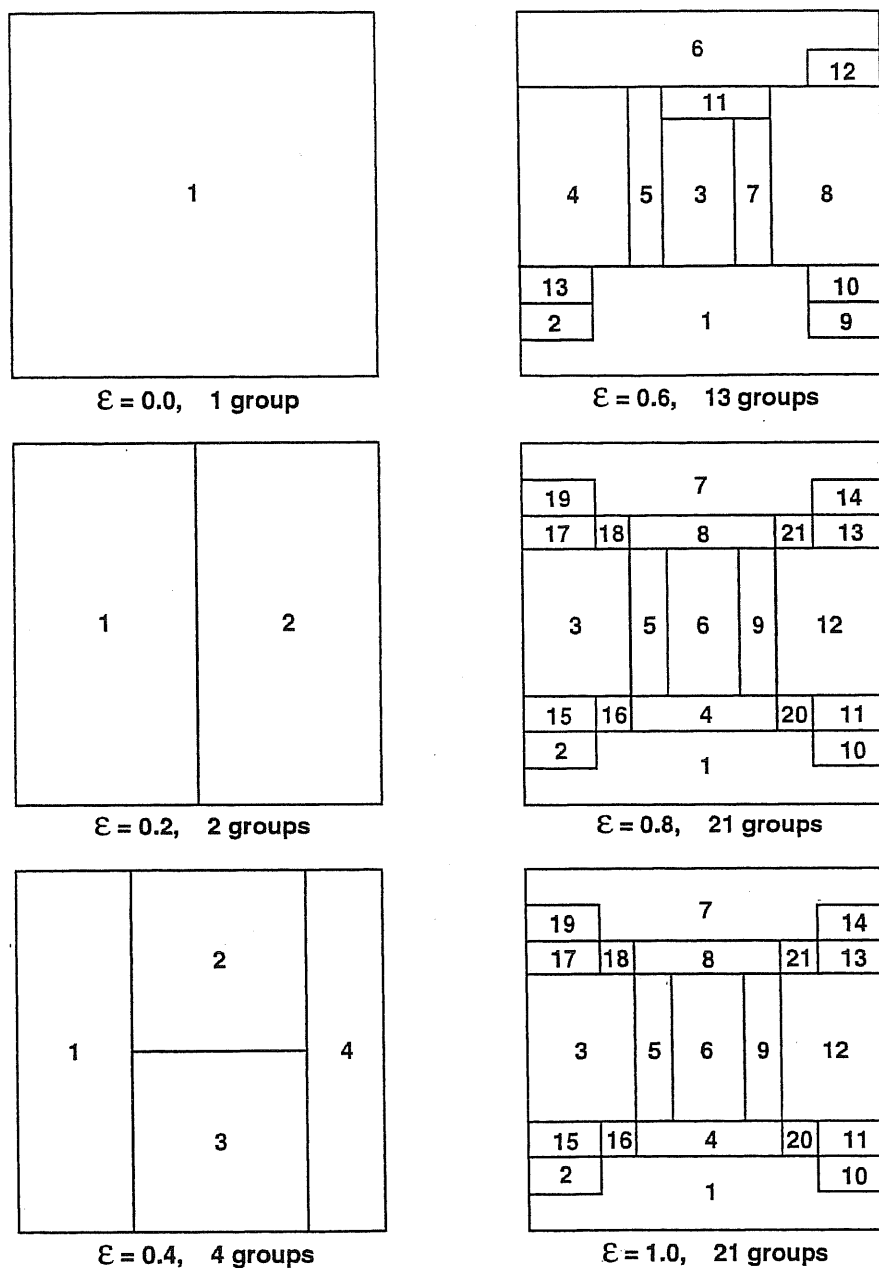The integral of the surface fluxes over the diurnal cycle is defined as

$$< F^i(g) > = 1/(T) \int_0^T f^i(g, t)dt$$

where

$$f^i(g,t)$$

is the time-dependent flux of slope/azimuth type i for group g and T is 24 hours. Applying this equation to the synthetic terrain results in diurnally integrated average fluxes for each group. Plots of the resulting average diurnal sensible and latent heat fluxes, as well as the Bowen ratios, over grasslands and evergreens for the 21 groups with a critical threshold of 1.0 are given in Figures 7a-7f for dry conditions and Figures 8 a-8f for saturated.

The integrated average sensible heat fluxes range from -3.3 to 58.8 W/m^2 for dry grasslands, and -85.6 to -33.3 for dry

$\mathcal{E} = 0.0$, 1 group

$\mathcal{E} = 0.6$, 13 groups

$\mathcal{E} = 0.2$, 2 groups

$\mathcal{E} = 0.8$, 21 groups

$\mathcal{E} = 0.4$, 4 groups

$\mathcal{E} = 1.0$, 21 groups

group number

Figure 4. (a) The decomposition and formation of homogeneous topographical groups for critical threshold values, ε, ranging from 0.0 to 1.0 with corresponding groups ranging from 1 to 21, and (b) the distribution of the corresponding slope/azimuth characteristic types for this synthetic surface (as defined in Fig. 2) with 1 km^2 land surface cell size.

evergreen woodlands. Similarly, the integrated average latent heat fluxes range from 52.6 to 60.9 W/m^2 for dry grasslands and 145.6 to 169.1 W/m^2 for dry evergreen forests. The very low values that are seen for groups 11 and 15 in Figures 7 and 8 correspond to the two steep north facing slopes that receive

a minimum amount of incident solar radiation. This is significant as this is an area where there will be a decreased snow melt rate during the spring and summer in mountainous regions. This indicates potential accumulation regions and will influence the surface runoff, the atmospheric surface
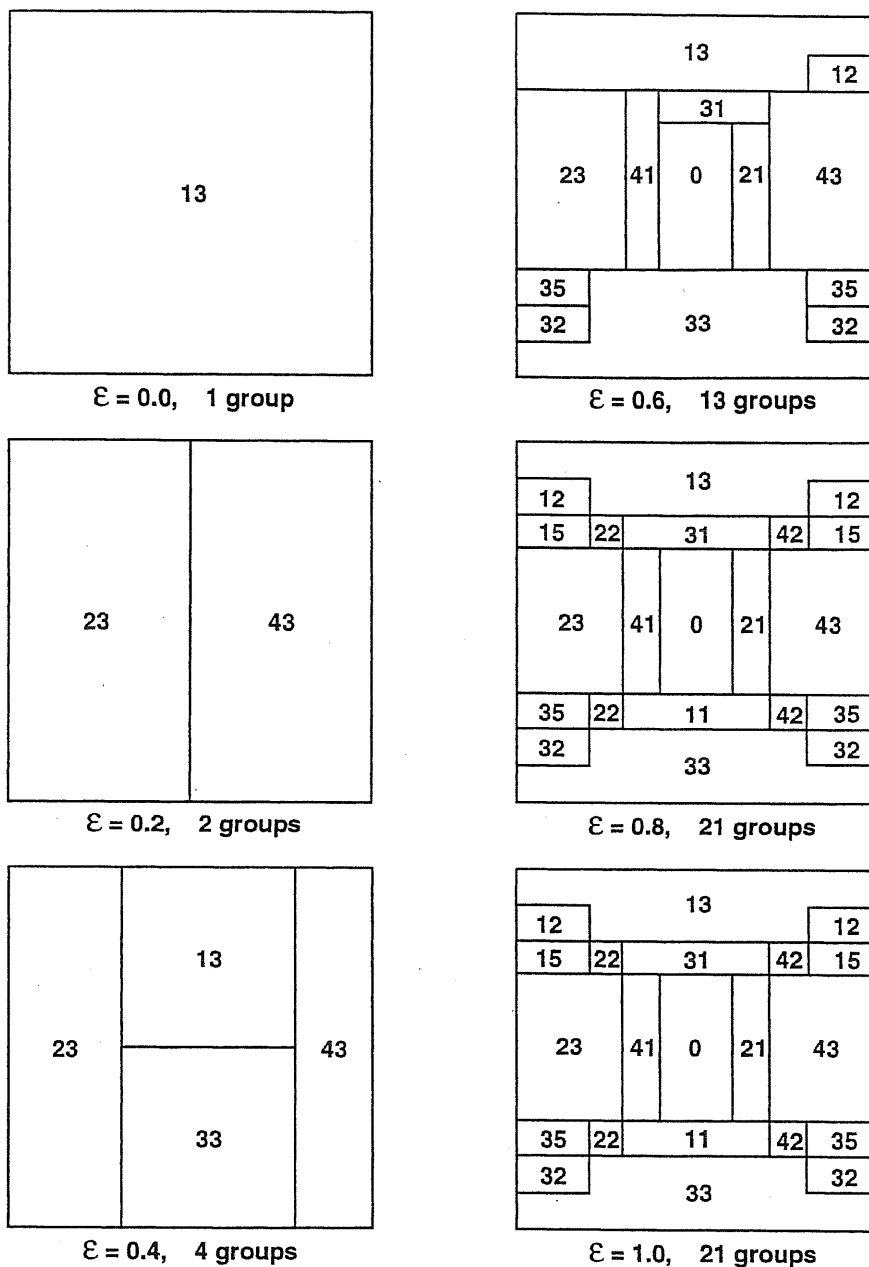
characteristic slope/azimuth type

Figure 4. (continued)

temperatures, and the surface albedo. The homogeneity scheme, as described in the appendix, provides information on the locations and areas of each group; this is an important and unique feature that will allow for improved hydrological simulations.

Extending this analysis further, area-weighted, diurnally averaged fluxes are defined as

$$< \overline{F^i} > = 1 /(A\ T) \int_o^T \int_1^G f^i(g, t)\ a(g)dgdt$$

where $a(g)$ is the area of group g and A is the total area of the AM grid cell, and it has been assumed that horizontal transport is negligible. This is true for nearly all cases, one exception is the lateral transport of water and nutrients that are carried with the runoff. This is to be accounted for in part by an application of the homogeneity algorithm. The area-weighted, diurnally averaged fluxes for this 100 km² area over grasslands are 47.7 W/m² and 58.8 W/m² for sensible and latent heats, respectively. Similarly, for evergreen forests the sensible and

INCIDENT SOLAR RADIATION
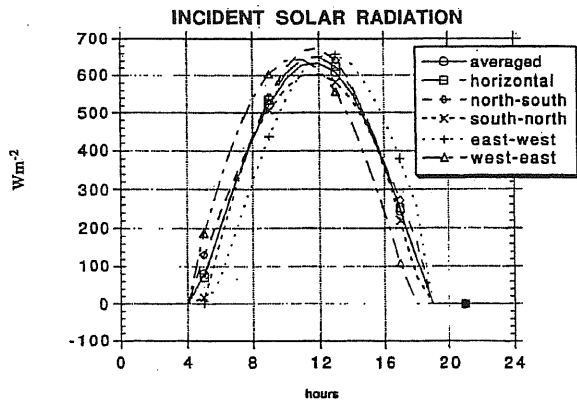
Figure 5. Plot of incident solar radiation at the surface for four surfaces each with a 10° slope and one which is flat.

latent heats are -43.2 W/m² and 164.8 W/m². The corresponding flat surface values over grasslands are 51.6 W/m² and 59.6 W/m² for sensible and latent heats. For evergreens the flat surface sensible heat flux is -40.37 W/m² and the latent heat flux is 167.0 W/m². The flat surfaces

overpredict the area-weighted sensible heat fluxes by 8% over grasslands and 6% over evergreens, while the latent heat is overpredicted by slightly more than 1%. This difference becomes greater than 20% for individual groups. Again, it should be noted that steeper slopes, higher latitudes, and a higher declination angle will significantly increase these percentages [Avissar and Pielke 1989].

Comparison Between 1 km x 1 km and 2 km x 2 km Land-Surface Cells

Increasing the cell size removes details from the topographic surface. In this section, a 2 km x 2 km description is used in place of the 1 km x 1 km resolution. In doing this, the input data essentially reads every other 1 km x 1 km grid point value and then an interpolation is performed. At a critical threshold of 100%, the resulting topographic types show the presence of the same watershed. The distribution has been reduced from 21 groups to 13 groups for this increased grid coarseness. Figures 9a and 9b respectively show the resulting slope/azimuth types and the distribution of groups for each type. Decomposition at this scale results in a single north facing group 1 and a single south facing group 2 in place of five groups for each of those regions (Figure 4a).
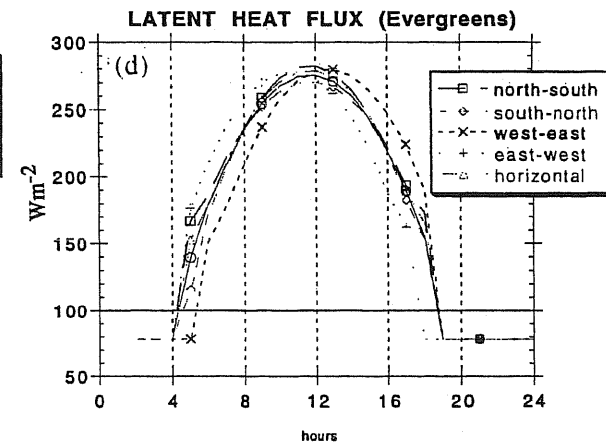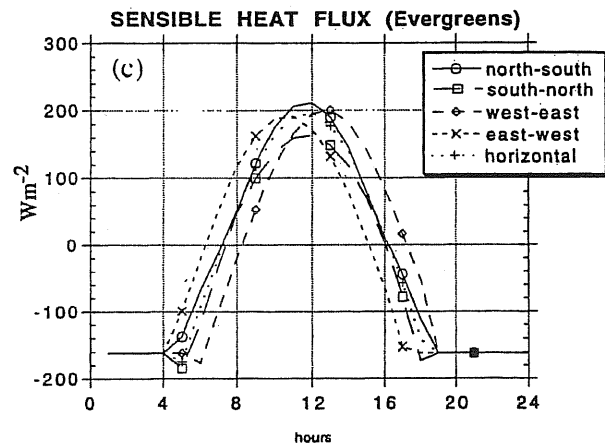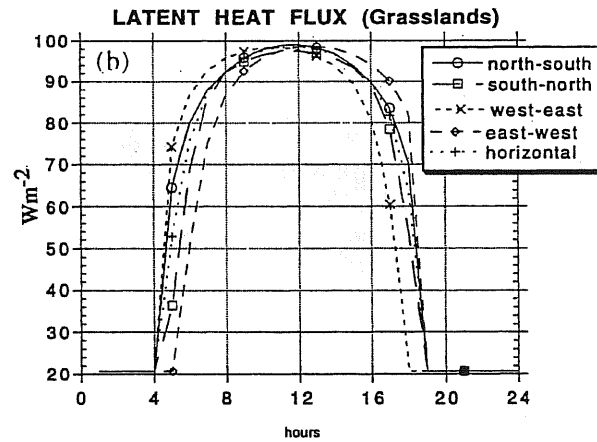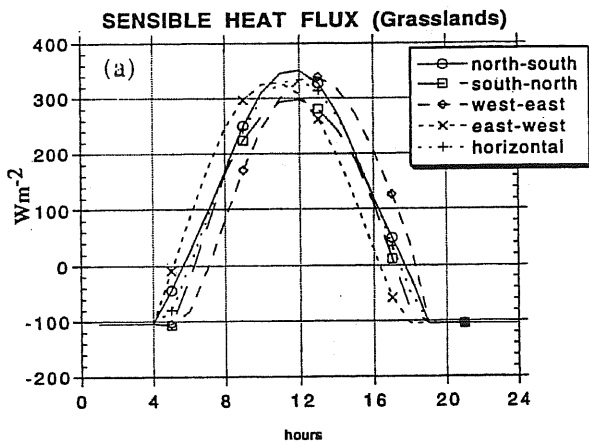

Figure 6. (a) Sensible heat flux over tall grass for the five surfaces as described in the text, (b) latent heat flux over tall grass, (c) sensible heat flux over evergreen woodland, and (d) latent heat flux over evergreen woodland.
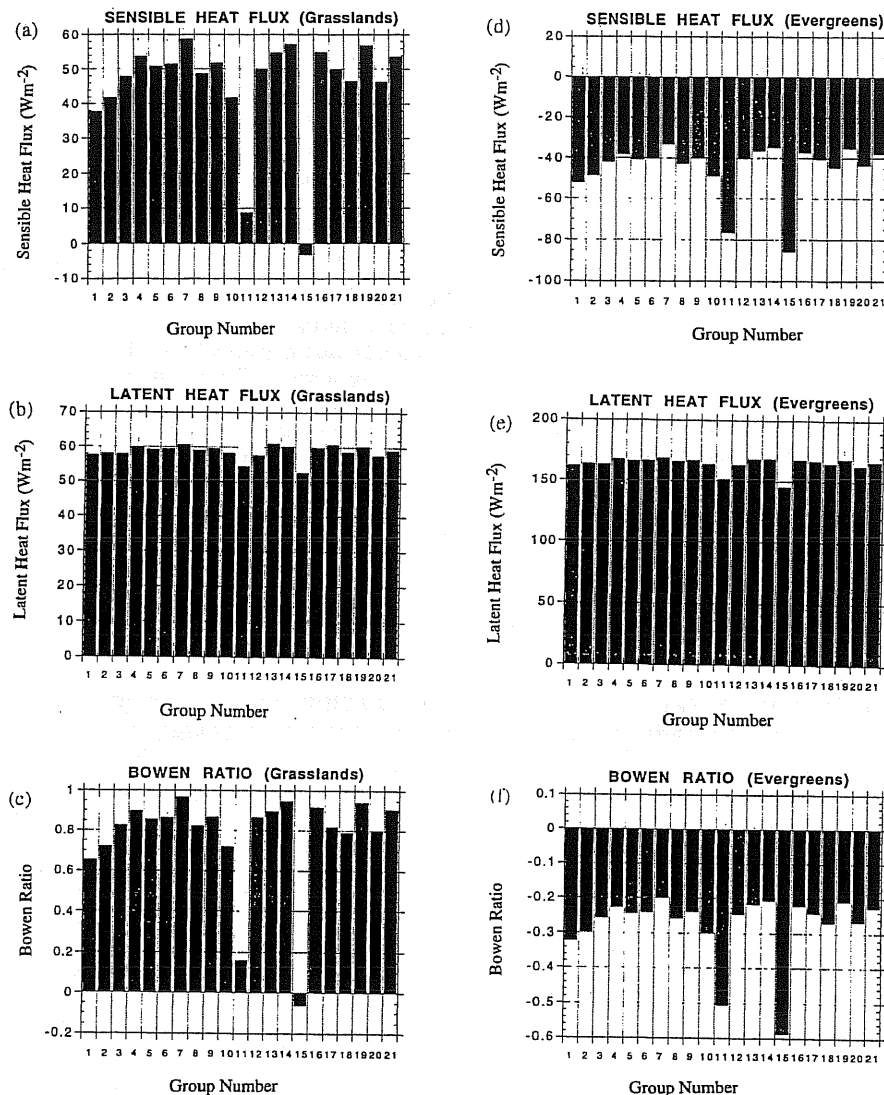
Figure 7. Diurnally integrated surface fluxes (as described in the text) for unsaturated land conditions with land surface cell resolution equal to 1 km² and $\varepsilon = 1.0$; (a) sensible heat flux over grasslands, (b) latent heat flux over grasslands, (c) Bowen ratio over grasslands, (d) sensible heat flux over evergreen woodlands, (d) latent heat flux over evergreen woodlands, and (f) Bowen ratio over evergreen woodlands.

Diurnally integrated surface fluxes and Bowen ratios over grasslands and evergreens are shown in Figure 10. The single north facing group (group 1) has a minimal sensible heat flux over both grasslands and evergreen forests, while the remainder of the surface has relatively uniform heating. The sensible heat flux over grasslands ranges from 20.4 to 56.9 W/m^2, while the latent heat flux ranges from 54.9 to 61.1 W/m^2. For evergreens, the sensible heat flux ranges from -66.2 to -34.4 W/m^2, and the latent heat flux ranges from 154.8 to 168.3 W/m^2. The diurnally integrated, area-weighted fluxes over grasslands are 43.5 W/m^2 for sensible heat flux and 58.3 W/m^2 for latent heat flux. The diurnally integrated, area-weighted fluxes over evergreens are -46.3 W/m^2 for sensible

heat flux and 162.9 W/m^2 for latent heat flux. This represents a slight underprediction from the 1 km x 1 km computation (Tables 2a and 2b).

The number of required groups depends on the scale of the land-surface model that is being implemented. For a community or landscape scale, the finest resolution may be needed. If a surface-vegetation-atmosphere transfer model, such as BATS, is to be coupled to a regional mesoscale meteorological model, then perhaps a coarser resolution may be sufficient. Lower resolution grids may satisfy the computational needs, depending on the degree of surface change. As the scales increase, the slope angles become less and less steep. A limit exists to this slope to scale
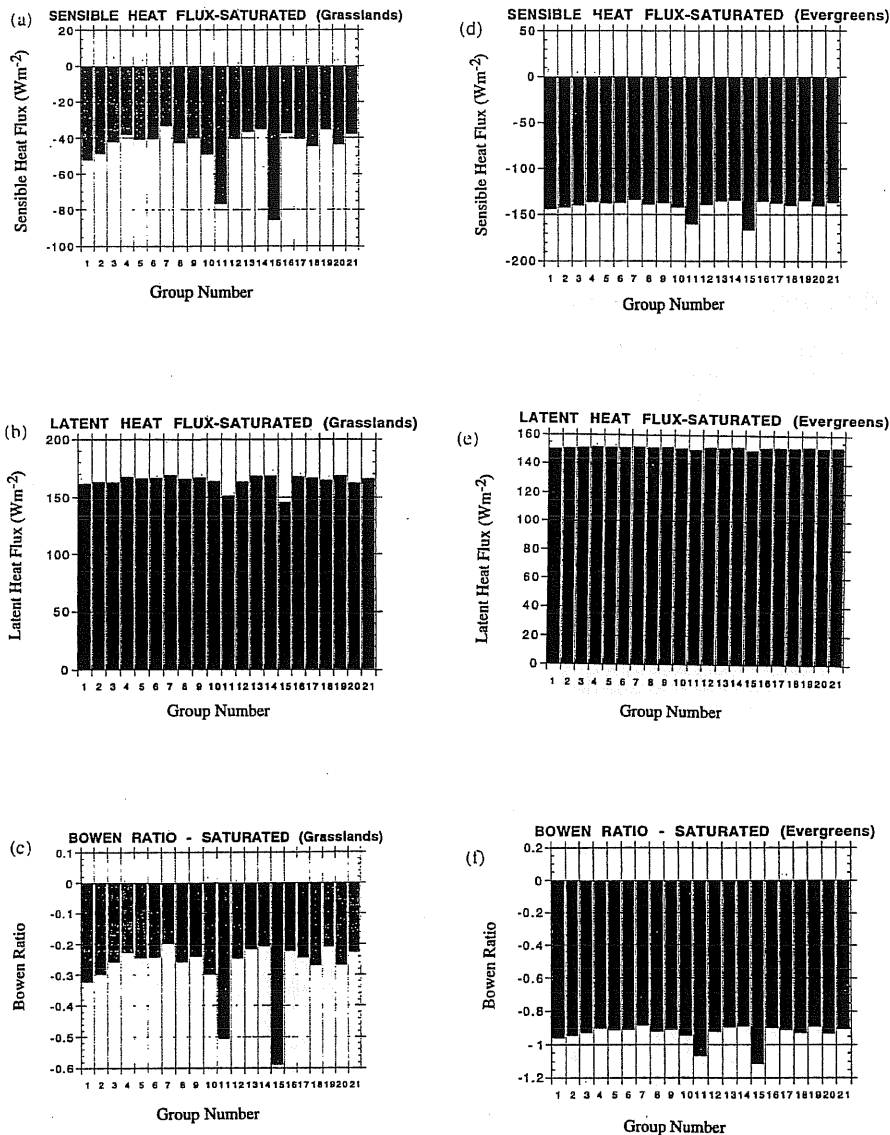
Figure 8. Diurnally integrated surface fluxes for saturated land conditions with land surface cell resolution equal to 1 km^2 ε = 1.0; (a) sensible heat flux over grasslands, (b) latent heat flux over grasslands, (c) Bowen ratio over grasslands, (d) sensible heat flux over evergreen woodlands, (e) latent heat flux over evergreen woodlands, and (f) Bowen ratio over evergreen woodlands

approximation after which everything will appear flat if it is exceeded. The scale where this blurring of topography occurs is approximately 1000 km^2.

Variations in the Critical Threshold

Up until now, ε was set to 100% for terrain sensitivity analysis and the input topographic data was exactly reproduced. There are cases where this may not be necessary, for example, when applying this technique to large scale general circulation models where land surface accuracy may be limited by computational efficiency.

Table 2a presents computed area-weighted, diurnally integrated surface fluxes for ε ranging from 0.0 to 1.0 for this synthetic terrain at the 1 km x 1 km resolution. It is seen that at about ε = 0.8, the degree of accuracy reaches 100% for this surface. These measures will be different for each set of characteristics and each surface that is investigated. The 100% value may be reached at an ε as low as 0.0 (e.g., over oceans, Figure A3), or at an ε as high as 0.99 for highly heterogeneous regions. For this synthetic topography, it is clear that for 100% accuracy, an ε value of 0.8 is most suitable. However, ε = 0.6 may be the most practical level of

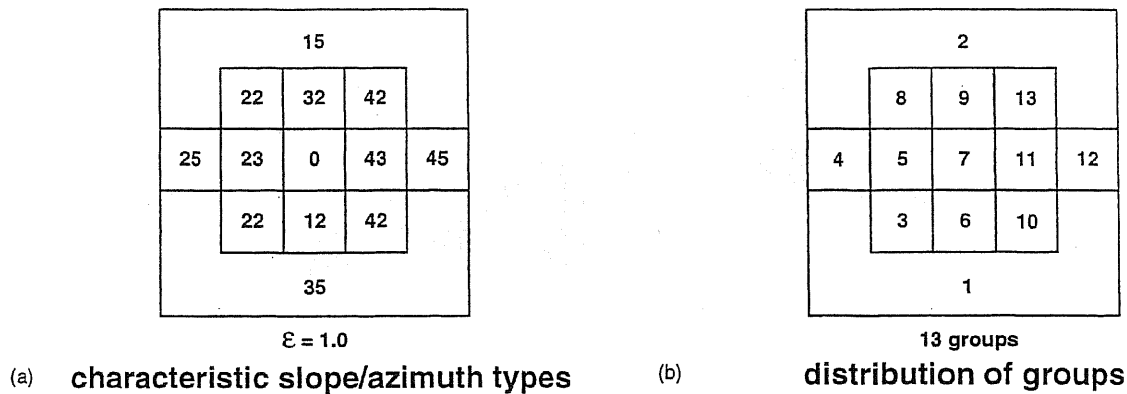(a) **characteristic slope/azimuth types**   (b) **distribution of groups**

Figure 9. (a) Decomposition and formation of homogeneous topographical groups for the synthetic terrain with a coarsened resolution of 4 km² per land surface cell and the critical threshold value set to 1.0. (b) Distribution of the corresponding homogeneous groups of slope/azimuth characteristic type.
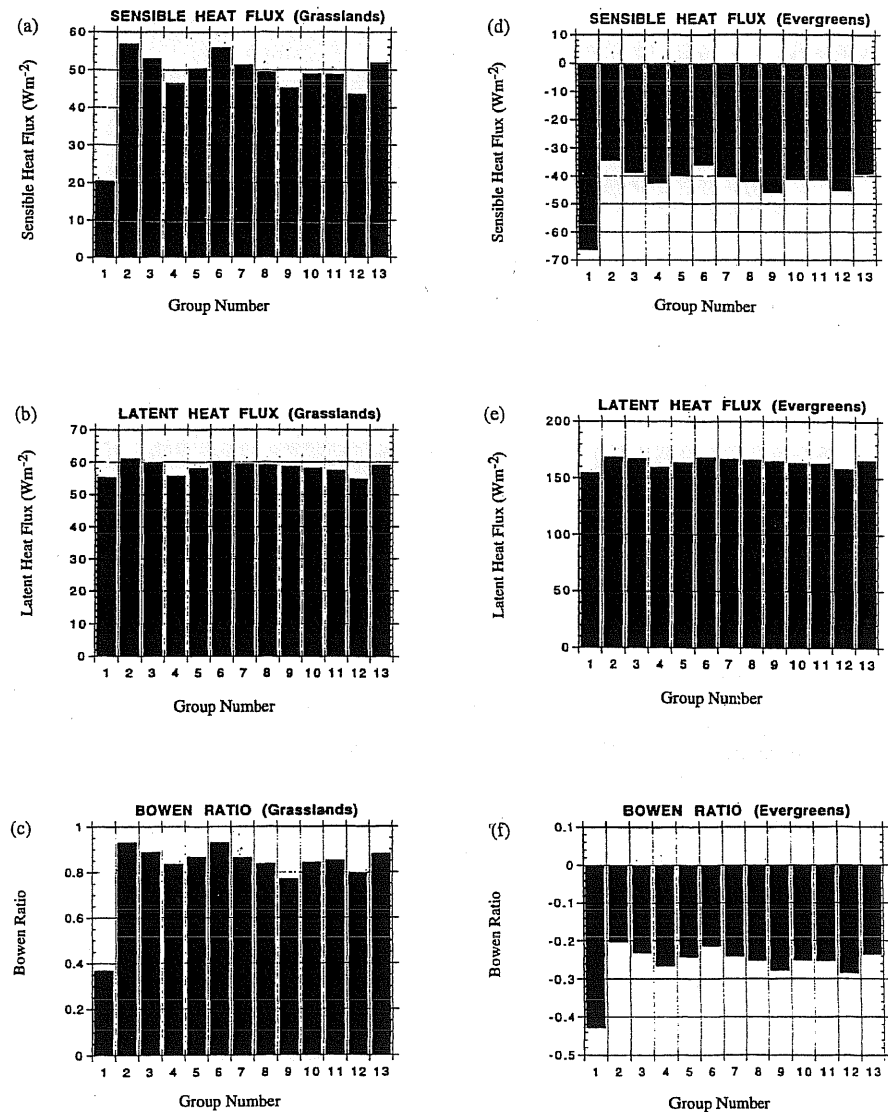

Figure 10. Diurnally integrated surface fluxes for unsaturated land conditions with land surface cell resolution equal to 4 km² $\varepsilon = 1.0$; (a) sensible heat flux over grasslands, (b) latent heat flux over grasslands, (c) Bowen ratio over grasslands, (d) sensible heat flux over evergreen woodlands, (e) latent heat flux over evergreen woodlands, and (f) Bowen ratio over evergreen woodlands.

Table 2a. Variations in Sensible Heat Flux, Latent Heat Flux, and the Bowen Ratio Over Grasslands and Evergreens as the Critical Threshold Ranges From 0 to 1

	0.0 Group 1	0.2 Group 2	0.4 Group	0.6 Group 3	0.8 Group 21	1.0 Group 21
			Grasslands			
$<\overline{S}>$	37.73	37.74	37.74	44.31	47.72	47.72
$<\overline{L}>$	57.72	57.72	57.72	58.13	58.81	58.81
$<\overline{\beta}>$	0.65	0.65	0.65	0.76	0.81	0.81
			Evergreens			
$<\overline{S}>$	-52.28	-52.28	-52.28	-45.94	-43.02	-43.20
$<\overline{L}>$	162.09	162.09	162.09	163.31	164.81	164.81
$<\overline{\beta}>$	-0.32	-0.32	-0.32	-0.28	-0.26	-0.26

Table 2b. Sensible Heat Flux, Latent Heat Flux, and Bowen Ratio Over Grasslands and Evergreens as Computed for Each of the 100 Land Surface Cells With the Critical Threshold Set to 1.0

Flat Surface (ε = 1.0)	Grassland	Evergreen
$<\overline{S}>$	51.58	-40.37
$<\overline{L}>$	59.60	167.04
$<\overline{\beta}>$	0.87	-0.24

accuracy, as the number of groups are reduced by 57% and this reduction translates linearly into an equivalent computational savings.

Table 2b indicates the flat surface sensible heat flux, latent heat flux, and the Bowen ratio for the 10 km x 10 km region. It is seen that at ε = 1.0, the percent change in the sensible heat flux, latent heat flux, and the Bowen ratio from a flat surface to the synthetic topography, $(\beta_{flat} - \beta_{topo}) / \beta_{flat}$, is given as 7.48%, 1.33% and 6.90%, respectively for grasslands. Similarly, for evergreens the percent change for sensible heat flux is -7.01%, latent heat flux is 1.34%, and the Bowen ratio is -8.33%. This implies that for mountainous terrain with slopes between zero and 20 deg., the sensitivity is less than 10%.

Computation of Topographic Groups for the California Sierra

Applying the results from above to real topography with assumed homogeneous evergreen vegetation (a 100 km^2 region with latitude 39.2°N near Lake Tahoe, California, Figure 11) sheds new light on the sensitivity of incident solar radiation on surface energy fluxes as a function of slope and azimuth. The elevation ranges from a minimum of 1800 to a maximum of 2600 m, with slope angles ranging from near flat to greater than 20°. The elevation data are from a digital elevation model and has a 90-m resolution. This 100 km^2 region was partitioned in the same fashion as above, where the topographic index ranges from 0 for flat up to 45 for a west facing slope with slope angle greater than 20°.

As in previous sections, a range of critical threshold values were used to compute Bowen ratios for a fixed vegetation. Figure 12 indicates the homogeneity decomposition of this surface for varying critical threshold values. At a threshold value of 1.0, there are 57 groups, at ε = 0.6 there are 43 groups, and at ε = 0.4, there are 21 groups. In going from ε = 1.0 to ε = 0.4, the coarse topographical structure is preserved; however, the detailed slope and azimuth are smoothed.

Figures 13a and 13b are histograms of diurnally integrated Bowen ratios for ε = 1.0 and 0.6, respectively. The north facing slopes which receive less radiation are cooler and emit less heat and thus have lower Bowen ratios than south facing or east or west facing slopes. This expected result shows the regions of potential snow accumulation as a function of incident radiation and topographic position. Other forcings such as orographic precipitation, vegetation patchiness, and surface roughness remain to be investigated in this fashion. Figures 13c and 13d indicate the product of the diurnally integrated Bowen ratio and the group area. This shows regions
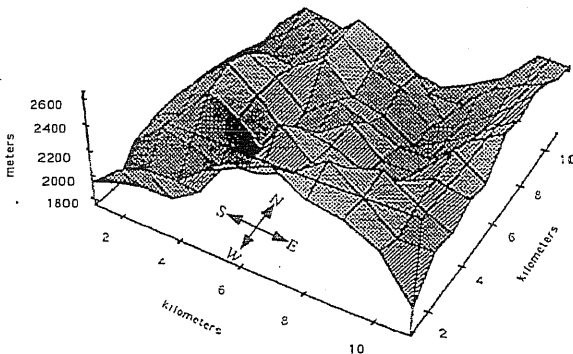
Figure 11. Topography for a 100 km^2 region in the Sierra near Lake Tahoe, California, based on DEM data.

characteristic types for each cell:

(grid a)

(a)

distribution of groups (57)

(grid c)

(c)   ε = 0.60

distribution of groups (21)

(grid b)

(b)   ε = 0.40

distribution of groups (43)

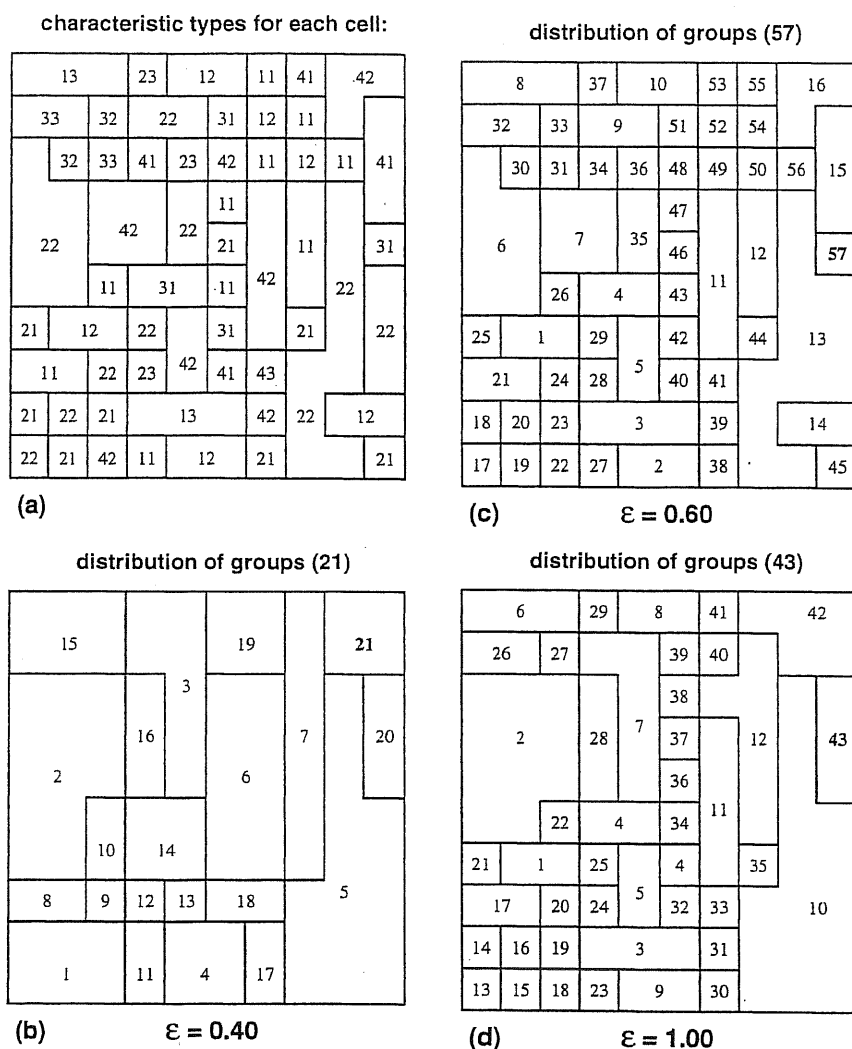(grid d)

(d)   ε = 1.00

Figure 12. (a) Characteristic terrain types for the Sierra region, (b) distribution of groups for a critical threshold of 0.40 resulting in 21 groups, (c) distribution of groups for a critical threshold of 0.60 resulting in 43 groups, and (d) distribution of groups for a critical threshold of 1.00 resulting in 57 groups.

that are most and least significant in a spatial sense as seen in Figures 12c and 12d.

Summing the product of the group Bowen ratio and the group area and dividing by 100 km^2 results in the area-weighted diurnally averaged Bowen ratio for this region. Figure 14 presents both the number of groups that are formed and a normalized Bowen ratio (the Bowen ratio at each critical threshold value divided by the Bowen ratio calculated for all 100 cells) plotted against critical threshold values ranging from 0.0 to 1.0. This includes the flat surface value (ε=0.0). The Bowen ratio for the 100 fine LSM cells are computed for their own slope and azimuth angles. The individual slopes and azimuths are used to compute the amount of available incident solar radiation for each LSM cell. From these results it is seen that the Bowen ratio of the flat surface is only 5% greater than the 1.0 critical threshold calculation for late spring at 39°N.

This low sensitivity value indicates that slope and azimuth are not as important as vegetation heterogeneity is to surface heat and moisture fluxes when the integrated net fluxes are considered. However, there is a significant subgrid effect where specific areas are being studied for local effects.

Conclusions

A simple topographic surface has been used here as an illustration of topographic decomposition and sensitivity. The results indicate that for June 6 the horizontal surface will overpredict the sensible heat flux over tall grass by approximately 8% and over evergreen woodland by 6%. The latent heat fluxes are less sensitive and indicate only about a 1% overprediction. Overestimated surface fluxes will cause errors in the input to atmospheric models by simulating
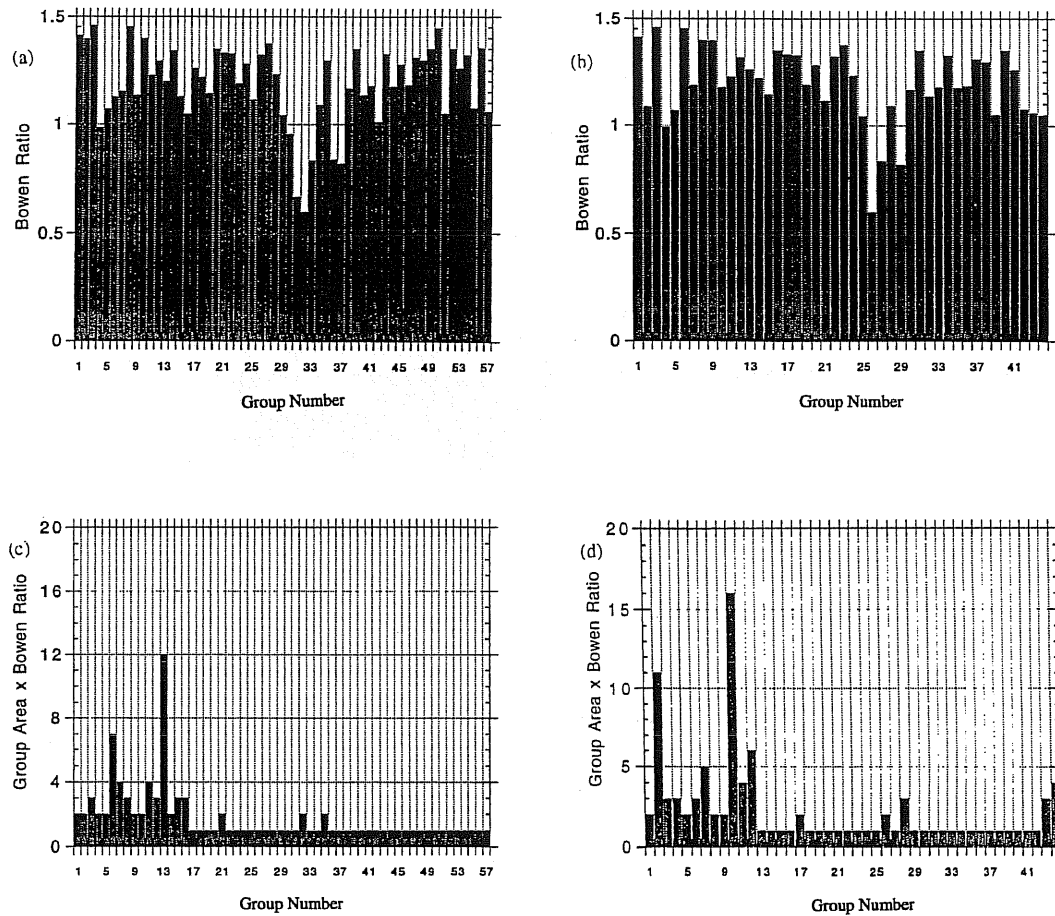
Figure 13. Histograms of the diurnally integrated Bowen ratio for the Sierra region with an assumed uniform evergreen woodland vegetation type at a critical threshold of (a) 1.00 and (b) 0.6. Histograms of the product of the diurnally integrated Bowen ratio with the group area for the Sierra region with an assumed uniform evergreen woodland vegetation type at a critical threshold of (c) 1.00 and (d) 0.6.

excessive heat and moisture fluxes to the lower atmosphere. It should be noted that a dry scenario has been imposed for this case study. One of the major impacts of slopes on surface fluxes is likely to be generated by the heterogeneity of water availability along the slope (water will drain to the lower part of the slope, creating a strong gradient of sensible and latent heat flux along a single slope with same azimuth and inclination). Steeper slopes for a range of latitudes with different degrees of surface wetness is being addressed in a follow-up study.

Digital elevation data from the Sierra mountains were used to determine levels of sensitivity of surface heat and moisture fluxes due to incident solar radiation forced by slope and azimuth. This calculation resulted in a Bowen ratio with a 5% difference between a surface which takes into account mountainous slope angles and azimuthal angles and that of an assumed flat horizontal surface. This small overestimation in the flat surface assumption indicates that surface heat flux response to incident solar radiation as forced by terrain is not very sensitive, except perhaps near deep canyons such as the Grand Canyon of northern Arizona. This will also be more significant for higher latitudes and lower sun angles, however.
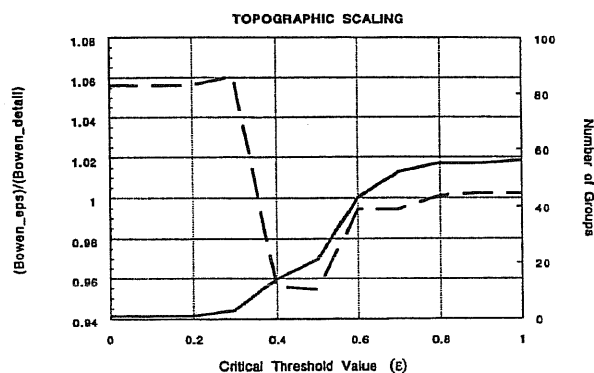

Figure 14. The left side ordinate (dashed line) represents the ratio of terrain forced to flat, area weighted diurnally averaged Bowen ratios for the Sierra region for a critical threshold value over the range 0 to 1. The right side ordinate (solid line) represents the number of groups formed for critical threshold values ranging from 0.0 to 1.0, where the flat surface value occurs at the critical threshold value 0.

While the results presented here are preliminary, the implications of this work extend beyond land-surface topographic sensitivity. This research is currently being expanded and implemented in a larger Earth system modeling framework. The homogeneity test is capable of decomposing and grouping data from a variety of sources and representations. The author is planning several studies utilizing this adaptive gridding technique to formulate watersheds, clouds, sea ice, and other geophysical features where a defined homogeneity is required. The resulting topographic groups that have been discussed here lend themselves to hydrological applications, as this characteristic type is being folded into the upstream area and soil conductivity using probability density functions to form a new hydrologic characteristic type. Formulation of a subgrid cloud parameterization based on applications of a temporal and spatial homogeneity criteria to observed and computed moisture fields is also being investigated.

The homogeneity algorithm has been rewritten as a C library with FORTRAN callable interfaces available as an object oriented code to provide decomposition of multiple characteristic types. The C version now has a quad-section option which partitions heterogeneous regions into fourths and thus preserves uniqueness of the solution (the current bisection may initiate latitudinally or longitudinally and can result in slightly different partitions). This algorithm will be used for product space studies to determine if an "effective" characteristic is suitable for this type of approach.

Appendix

Homogeneity Testing Algorithm

Intuitive initializations for characteristic land surface partitioning may work for a specific class of problems; for example, where it is known that the surface characteristics are constant in time. However, accurate simulation of surface processes demands time varying surface types. Furthermore, decomposition of surface characteristics into homogenous or nearly homogenous groups can only be approached through a combination of objective partitioning and statistical approximations.

This appendix discusses an objectively derived dynamic adaptive gridding technique that depends only on the available temporally and spatially varying input data. This technique can be applied initially and used to update and reformulate grids at any specified time. A homogeneity theory is presented and an application to vegetation characteristics is provided as an example of the utility of this technique [*Miller and Foster*, 1991; *Miller*, 1993b, 1994]. As mentioned in the main text, a number of researchers have previously investigated aspects of this problem [e.g., *Andre et* al., 1990; *Mahrt*, 1987; *Avissar and Pielke*, 1989; *Pielke et al.*, 1991; *Lee et al.*, 1991; *Dalu and Pielke*, 1991; *Pielke et al.*, 1993; *Avissar*, 1991; *Miller*, 1993a].

Theory

The adaptive grid requires a finite difference grid composed of cells at the land surface that maintain a match with the overlying atmospheric mesh which provides climate forcing and feedbacks. The overlying cell is defined here as the large-scale or atmospheric model cell, AM, and may be representative of any atmospheric scale grid cell. Land surface characteristic data is input and updated on a much smaller

scale. The fine mesh land surface input data may be a description of surface vegetation types, soil textures, topography, nutrients, and/or some effective combination that is representative of the domain. This cell is defined as the
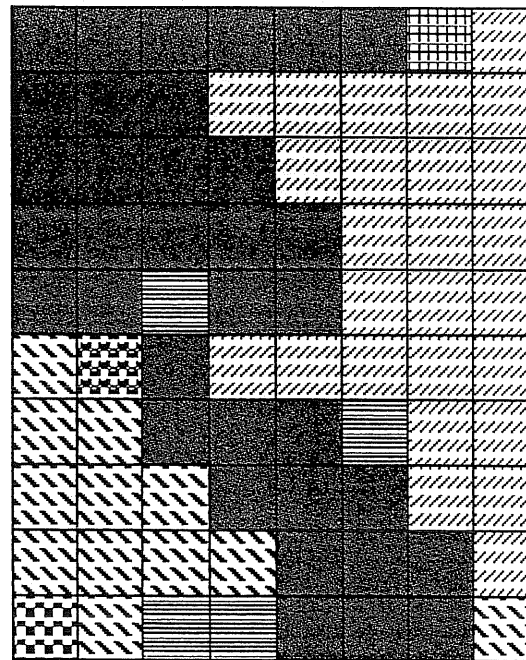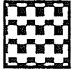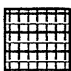

VEGETATION TYPE		NUMBER OF CELLS
	Evergreen Woodland	4
	Evergreen Thickets	1
	Shrubs	1
	Short Grass with Meadows	34
	Tall Grass with Shrubs	1
	Tall Grass	12
	Medium Grass	27

Figure A1. An 8° x 10° AM cell with coordinates centered at 115W and 45N. Of the eighty 1° x 1° characteristic vegetation cells, 34 are short grass with meadows, 27 are medium grass, 12 are tall grass, 1 is tall grass with shrubs, 4 are evergreen woodland, 1 is evergreen thickets, and 1 is shrubs.

land surface model cell or the LSM cell. The adaptive gridding technique converts the fine-scale, possibly a heterogeneous surface of characteristics, into a set of groups of homogeneous types.

The criterion by which a group is deemed homogeneous is based on a simple tolerance parameter which the user controls. The technique reduces the number of unique subregions within the AM cell on which calculations must be performed, thereby reducing the required computational work, frequently by more than an order of magnitude.

In the formulation of homogeneous groups, an intermediate set of regions is needed to keep track of the location, mass, and energy. A region or block consists of LSM cells, is rectangular in shape, and may range in size from a single LSM cell to the entire AM cell. All energy and mass are conserved, as there is a conservation of area and thus there are no net losses or gains from the system.

Homogeneity is specified by a threshold criteria (ε) and ranges from 0.0 to 1.0. For a given ε, each region is evaluated for its percent uniformity. Percent uniformity is the frequency of occurrence of the most dominant characteristic type within the region. If the percent uniformity is equal to or greater than ε, then the region is labeled homogeneous with the dominant characteristic type. If the percent uniformity is less than ε, then the region is labeled heterogeneous and bisection occurs. The advantage of a threshold criteria is that different scales of sensitivity can be investigated and computations can be made even more economical by decreasing ε to a value where the surface response is essentially unchanged from the more accurate surface descriptions than a larger ε would provide.

An initial region is defined as the AM cell, if the criteria threshold is not satisfied then heterogeneity is computed. The initial region is bisected either latitudinally or longitudinally depending on the initialization (the C version of the homogeneity test now runs with quad-section to maintain uniqueness of the solution), and two newly formed regions are produced from the initial region. Each of these newly formed regions are then separately evaluated for homogeneity. This procedure continues forming smaller and smaller regions, replacing a heterogeneous region, until homogeneity is attained or regions equivalent to the LSM cell remain.

The strongest feature of this approach is the ability to investigate and determine what level of accuracy is required for a specific problem. A partial derivative of the surface function with respect to the level of accuracy may be used to determine what minimum fraction of ε is required. The following is an application of characteristic vegetation based on the homogeneity test.

Application

Figure A1 demonstrates an AM cell with a heterogeneous surface composed of 80 LSM cells with coordinates centered at 115°W and 45°N. Global characteristic vegetation data are used here as an application of the homogeneity test. Matthews (1983) provides data on vegetation types for a global 1° x 1° resolution with 32 vegetation type classes. This data set acts as a static characteristic surface type input for the determination of homogeneous regions and groups that are needed to describe each large scale cell. A coarse scale 8° x 10° resolution is chosen here for the AM cell. This resolution implies that a maximum of seven bisections can occur before the minimum 1° x 1° LSM is reached. Below this minimum

resolution, a statistical aggregation up to 1° x 1° is required for homogeneity.

These input data indicate that there are 34 short grass LSM cells that are meadows, 27 are medium grass, 12 are tall grass, 1 is tall grass with shrubs, 4 are evergreen woodlands, 1 is evergreen thickets, and 1 is shrubs. The number of resulting homogeneous regions and groups are dependent on the connectedness of the LSM cells of the same type and the required threshold criteria. That is, LSM cells that have the same characteristic type and share an edge but not strictly a corner, are considered to be of the same region. Similarly, regions with the same type that share an edge, but not strictly a corner, are of the same group.
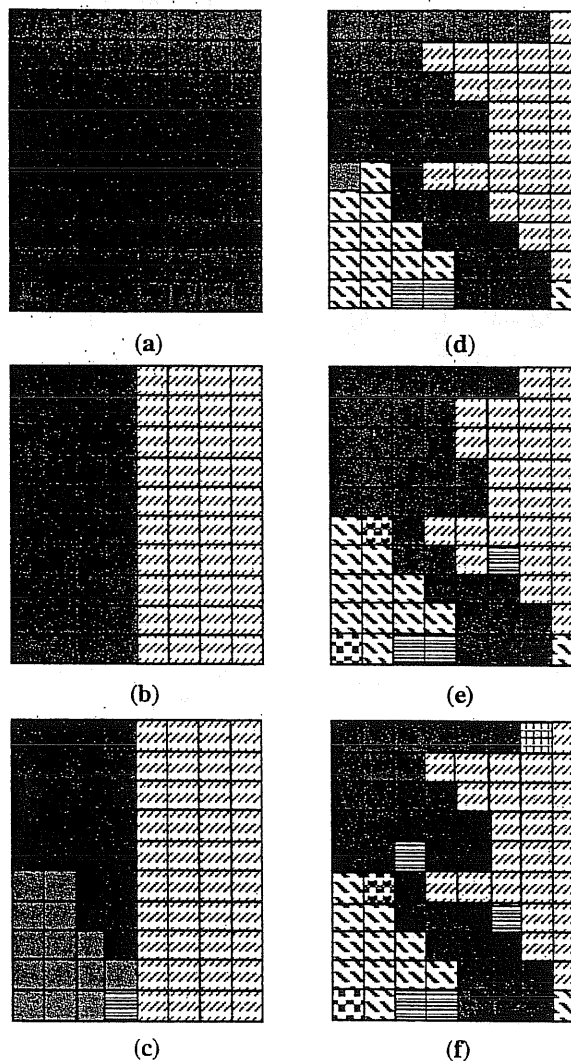

Figure A2. (a) For the threshold criteria, ε, less than 0.425, only one cell is needed to meet the homogeneity test, (b) for ε = 0.425, the homogeneity criteria is not met with one cell and an initial bisection takes place, resulting in two cells and two groups, one with short grass and one with medium grass, (c) for ε = 0.60, there need to be eight cells and four groups, (d) for ε = 0.80, 29 cells and six groups result, (e) for ε = 0.90, 35 cells and eight groups result, and (f) for ε = 1.00, 45 cells and 11 groups result.
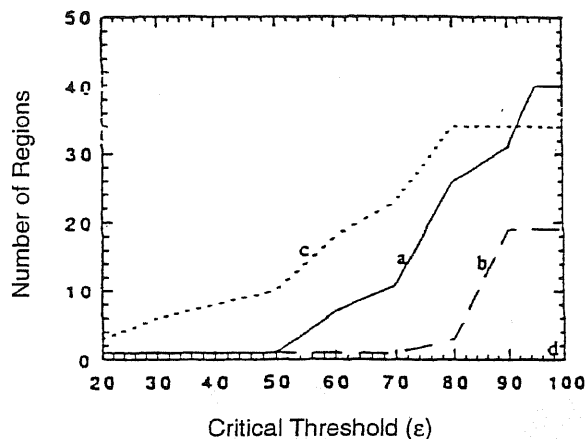
Figure A3. Plot of number of vegetation regions against a threshold or minimum criteria, ε, for (a) midlatitude grasslands, (b) Brazilian rain forest, (c) coastal boreal lowlands, and (d) oceans.
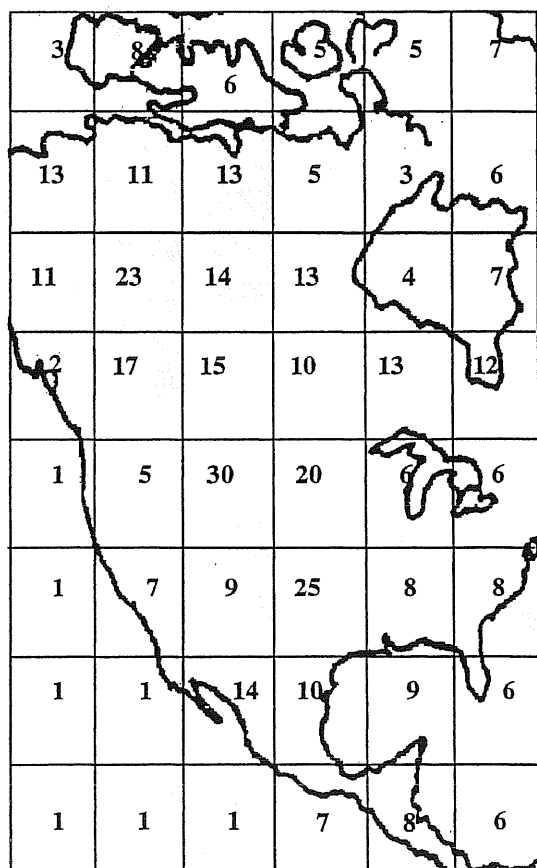
Figure A4. *Matthew's* [1983] characteristic vegetation is mapped over an array of 8° x 10° grid cells over the region 130W to 80W by 6N to 70N. The homogeneity forms groups for each 8° x 10° grid cell reducing the number of homogeneous regions by approximately an order of magnitude while maintaining 100% accuracy.

Figure A2a indicates that for ε less than 0.425 only one region is required to meet the homogeneity test, this region consists of all 80 LSM cells. When ε equals 0.425, the homogeneity criteria is not met and an initial bisection takes place resulting in two regions and two groups, one with short grass and one with medium grass (Figure A2b). At ε = 0.60, there are eight regions and four groups (Figure A2c), ε = 0.80 results in 29 regions and six groups (Figure A2d), ε = 0.90 results in 35 regions and eight groups (Figure A2e), and when the threshold criteria is 1.00, 45 regions and 11 groups result (Figure A2f). The resulting 11 groups at this finest breakdown represent separate homogeneous regions for each of which a land surface calculation can be made. Such a breakdown will vary from location to location depending on the degree of inherent homogeneity. That is, an 8° x 10° AM cell in the middle of an ocean will result in a single region and a single group regardless of the threshold criteria and an AM cell which includes coastlines and/or urban areas will require a higher number of homogeneous groups covering smaller regions (Figure A3).

Application of this approach to global calculations is illustrated in Figure A4. In this case, the characteristic vegetation data [*Matthews* 1983] are used for the North American continent with 8° x 10° AM cells. It is seen from Figure A4 that a threshold criterion of ε = 1.00 can be maintained while the actual number of homogeneous groups is approximately an order of magnitude lower than the 80 LSM cells per AM grid cell initially required. The initial application of this approach indicates the potential computational savings that will be available when using more detailed LSM characteristics. The addition of ecophysiology, biogeochemistry, and hydrology will add to the required amount of computational time spent at each AM subcell, and the use of homogeneous subgrid regions will become increasingly important as surface models become more complex.

The homogeneity algorithm has also been applied to subgrid sensitivities of latent and sensible heat fluxes due to heterogeneous vegetation and cloudiness over the FIFE study site [*Miller* 1993b].

References

Andre, J.-C., P. Bougeault, and J.-P. Goutorbe, Regional estimates of heat and evaporation fluxes over non-homogeneous terrain. Examples from the Hapex-Mobilhy Programme. *Boundary Layer Meteorol., 50*, 77-108, 1990.

Avissar, R., A statistical-dynamical approach to parameterize subgrid-scale land-surface heterogeneity in climate models in *Land Surface-Atmosphere Interactions for Climate Modeling: Observation, Models, and Analysis*, edited by E. F. Wood, O. O. Kluwer Academic, Norwell, Mass., 1991

Avissar, R., and R.A. Pielke, A parameterization of heterogeneous land surfaces for atmospheric numerical models and its impact on regional meteorology, *Mon. Weather Rev., 117*, 2113-2136, 1989.

Dalu, G.A., and R.A. Pielke, Vertical heat fluxes generated by mesoscale atmospheric flow induced by thermal inhomogeneities in the PBL, *J. Atmos. Sci.*, 1991.

DeBoor, C., A Practical Guide to Splines, pp. 346-350, Springer Verlag, New York, 1978.

Dickinson, R.E., A. Henderson-Sellers, P.J. Kennedy, M.F. Wilson, Biosphere-Atmosphere Transfer Scheme (BATS) for the NCAR

Community Climate Model, *Tech. Note, NCAR/TN-275+STR*, 69 pp. Natl. Cent. for Atmos. Res., Boulder, Colo., 1986.

Kondrat'yev, K.Y., *Actinometry*. NASA, Washington, D. C. , N66-10158, 512 pp., 1965.

Lee, T.J., R.A. Pielke, T.G.F. Kittel, and J.F. Weaver, Atmospheric modeling and its spatial representation of land surface characteristics, paper presented at First International Conference/Workshop on Integrating GIS and Env. Mod., Boulder, Colo., Sept. 15–19, 1991.

Marht, L., Grid-averaged surface fluxes, *Mon. Weather Rev.*, 115, 1550-1560, 1987.

Matthews, E., Global vegetation and land use: New high resolution data bases for climate studies. *J. Clim.*, 2, 474-487, 1983.

Miller, N.L., and I.T. Foster, Hierarchical framework for coupling a biogeochemical trace gas model to a general circulation model, *Contrib. 26*,. Argonne Nat. Lab., Environ. Res. Div., 1991.

Miller, N.L., The hierarchical systems flux scheme: The homogeneity test, in *Conference on Hydroclimatology*, pp. 36–40, American Meteorology Society, Boston, Mass., 1993a.

Miller, N.L., Applications of a hierarchical systems flux scheme for interactively coupling subgrid land surface models with atmospheric general circulation models, *Rep. UCRL-JC-114100*, Lawrence Livermore Nat. Lab., Global Climate Res. Div., 1993b.

Miller, N.L., A homogeneity grouping technique for geophysical climate models, *Rep. UCRL-JC-115996*, 1994.

Pielke, R.A., G.A. Dalu, J.S. Snook, T.J. Lee, and T.G.F. Kittel, Nonlinear influence of mesoscale land use on weather and climate, *J. Clim.*, 4, 1053-1069, 1991.

Pielke, R.A., G.A. Dalu, T.J. Lee, H. Rodriguez, J. Eastman, and T.G.F. Kittel, Mesoscale parameterization of heat fluxes due to landscape variability for use in general circulation models. Exchange Processes at the land surface for a range of scales. Proceedings of the Yokohama Symposium, July 1993, *IAHS Publ. 212*, 331-342, 1993.

N. Miller, Global Climate Research Division, Lawrence Livermore National Laboratory, P.O. Box 808, Livermore, CA 94550. (e-mail: norm@llnl.gov)